FISEVIER

Contents lists available at ScienceDirect

Journal of Structural Geology

journal homepage: www.elsevier.com/locate/jsg



Comparison of brittle- and viscous creep in quartzites: Implications for semibrittle flow of rocks



Jacqueline E. Reber^{a,*}, Matej Pec^b

- ^a Department of Geological and Atmospheric Sciences, Iowa State University, Ames, IA 50011, USA
- ^b Department of Earth, Atmospheric and Planetary Sciences, Massachusetts Institute of Technology, Cambridge, MA 02139, USA

ABSTRACT

The co-existence and interaction between brittle and viscous deformation processes contributes to the integrated strength of the crust and results in a wide range of energy-release mechanisms ranging from earthquakes to creep. Here, we compare flow laws derived for quartz-rich rocks deforming by brittle creep, wet dislocation power-law creep and dissolution-precipitation creep. We investigate theoretically the conditions when both brittle and viscous processes contribute significantly to deformation provided that all processes act independently and in parallel. Utilizing a comprehensive data set for deformation experiments in quartz-rich rocks, we find that the transition between deformation mechanisms is strongly dependent on input variables such as initial flaw size and grain size. The transition can occur abruptly or over hundreds of MPa in differential stress and hundreds of degrees Kelvin at a constant strain rate. The transition is strongly dependent on grain-size and confining pressure. Limitations to this work are first that all three flow laws are poorly constrained by experimental data for conditions relevant for the comparison. Secondly, a need exists for new experiments to infill the knowledge gaps between high-temperature and low-temperature deformation experiments and deriving quantitative flow laws for low-temperature plasticity and high-temperature brittle creep.

1. Introduction

Constraining the rheological behavior of the crust is of fundamental importance for understanding of large-scale tectonics as well as small-scale processes related to earthquake generation. This task, however, is exceedingly difficult because the crust is comprised of many lithologies and deformation occurs over a broad range of pressures, temperatures, and strain rates. Therefore, a variety of deformation mechanisms contribute to the integrated strength of the crust. To add to the complexity of the situation, the strength of rocks is greatly influenced by the presence of fluids and evolves with deformation, as for example, different deformation mechanisms will dominate in intact rocks as compared to fault rocks in mature fault zones. Consequently a strain-dependent evolution of the strength of the crust is to be expected (e.g. Evans, 2005).

In this paper, we limit ourselves to exploring the deformation behavior of low-porosity, quartz-rich rocks at low strains so that the porosity can be expected to remain approximately constant during deformation and no significant strain localization occurs. We will use the terms *brittle* when deformation is mediated by fractures and *viscous* when deformation is mediated by dislocations and/or diffusive mass

transfer as elaborated in more detail below.

1.1. Deformation mechanisms in the brittle and viscous fields

Brittle processes involve crack nucleation and growth through the breaking of atomic bonds and formation of new surfaces that ultimately lead to frictional sliding. Brittle deformation is accompanied by an inherent need for dilatancy as new cracks open and individual fragments slide past each other i.e. do work against the confining pressure.

Temperature-activated viscous processes involve the motion of atomic disorder within a crystal lattice as well as material transport in a fluid phase (Fig. 1). Viscous deformation exhibits a strong dependence of steady-state stress on strain rate as well as temperature and is largely independent of confining pressure at crustal conditions. The deformation is volume conserving and dependent on atomic mobility, hence temperature and time. At low-stress conditions, diffusion creep is usually the dominant deformation mechanism in rocks. Stress is linearly dependent on strain rate and further depends on grain size (i.e. diffusion distance). A special case of diffusion creep is dissolution-precipitation creep, where the flux of atoms is mediated by a liquid phase on grain boundaries (Gratier et al., 2013; Klinge et al., 2015). At higher

E-mail address: jreber@iastate.edu (J.E. Reber).

^{*} Corresponding author.

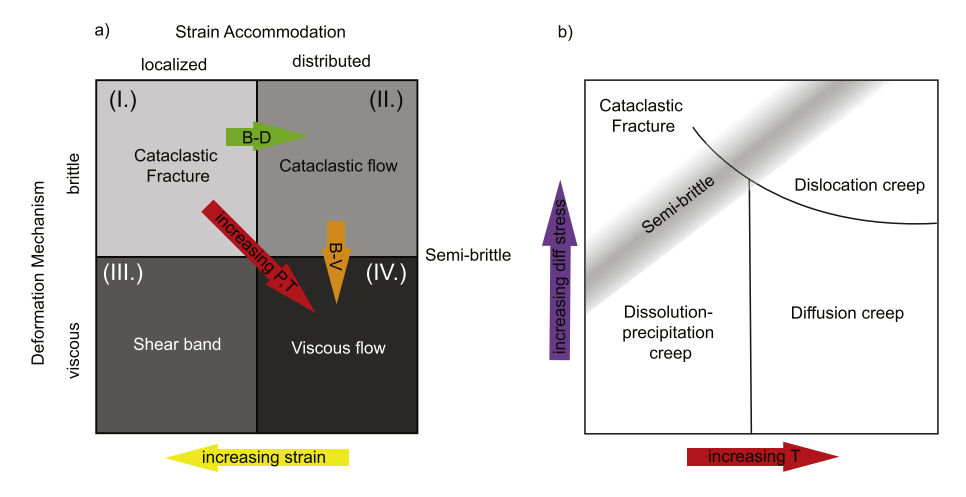


Fig. 1. a) Transitions which may occur in a deforming rock (modified after Rutter (1986)). B-D stands for brittle-ductile transition, B-V stands for brittle-viscous transition. b) Schematic representation of the different deformation mechanisms and their relative temperature and differential stress conditions (modified after Davis et al. (2012)).

stresses, materials deform by dislocation mechanisms in the power-law creep regime. Strain rate is proportional to stress with a stress exponent of 3–5 and shows no dependence on grain size. At even higher stresses, dislocation glide with negligible climb out of the slip planes accommodates strain in the low temperature plasticity regime (see Kohlstedt and Hansen (2015) for a review of viscous deformation).

1.2. Deformation mechanisms in the semi-brittle field

Semi-brittle flow occurs when viscous and brittle deformation mechanisms contribute coevally and significantly to strain accommodation during deformation. Hence micro-mechanically, semi-brittle deformation would be expected to exhibit a pressure dependence due to dilatation, as well as a temperature and strain-rate dependence due to the temperature-activated motion of defects and atoms. Brittle and viscous processes act either sequentially or simultaneously. For example of serial semi-brittle deformation is when fracturing produces fine-grain sizes that then deform by fluid-assisted diffusion creep (brittle - > viscous) (Fusseis and Handy, 2008; Gratier et al., 1999; Menegon et al., 2013; Trepmann and Stöckhert, 2003). An example of parallel semibrittle deformation is when one phase deforms by fracturing while another phase deforms by viscous flow in a polyphase rock (Handy, 1990; Jammes et al., 2015). Brittle and viscous deformation can occur simultaneous in a single mineral phase (Fredrich et al. 1989, Hirth and Tullis, 1994, Nicolas et al., 2016; Onasch, 1994) as well as in a polyphase rock (Fagereng et al., 2014; Handy, 1990, 1994; Jammes et al., 2015; Marti et al., 2017; Nevitt et al., 2017; Pec et al., 2012a, 2016; Platt, 2015; Violay et al., 2012).

The study of brittle and viscous properties of rocks have led to a variety of phenomenological flow laws, which describe the deformation of rocks for specific stress, pressure, temperature, grain size, porosity, etc. conditions. The flow laws describing diffusion creep were first developed by Nabarro (1948), Herring (1950) and Coble (1963). The flow laws describing dislocation creep were developed by several researchers during the 1950's (Mott. 1951; Weertman, 1955) and are well-tested and established equations to calculate the steady-state strain rate as a function of a number of external and internal variables at high homologous temperature. More recently Ashby and Hallam (1986), Ashby and Sammis (1990), Bhat et al. (2012), and Brantut et al. (2012) developed a continuum-mechanical flow law to describe secondary brittle creep. Even though this flow law is not derived for a steady state condition, the similar continuum-mechanic formulation allows for a comparison of several flow laws and a theoretical investigation of the respective contribution to total strain rate provided that the mechanisms act independently and in parallel. In this paper, we seek to compare flow laws for brittle creep with wet dislocation power-law creep and a dissolution-precipitation creep to investigate theoretically the conditions when we would expect the co-existence of brittle and viscous behavior in one mineral phase. We attempt to quantify the contribution of individual micro-mechanisms to the bulk deformation and to identify regions in stress – temperature space where most interplay would be expected to inform future experiments and field studies aimed at elucidating the brittle – viscous transition in low porosity rocks. In this contribution, we will concentrate on the brittle - viscous transition in quartz-rich rocks with $\rm H_2O$ fluid present as they have the largest amount of experimental data available.

2. Experimental data

We surveyed the literature and collected rock-deformation experimental data about wet quartzites and low-porosity (< 10%) quartz sandstones published over approximately the last thirty years in gasmedium, fluid-medium, and solid-medium deformation apparatuses using weak salts (Appendix Table A1 or an electronic copy is at https://zenodo.org/record/1256838#.WxA3oKkh2hY). Our main focus is on deformation experiments that were conducted at elevated temperatures on low-porosity rocks, and the reader is referred to Brantut et al. (2013) for an extensive list of lower temperature, higher porosity experiments. The only constant parameter in our collection is the dominance of quartz compositionally. The experimental procedure, rock type and purpose of the experiment vary between the individual studies (Appendix A1). Strain rates in general shear experiments were converted to equivalent strain rates as

$$\dot{\varepsilon} = \frac{\sqrt{3}}{3} \dot{\gamma},\tag{1}$$

where $\dot{\varepsilon}$ is equivalent strain rate and $\dot{\gamma}$ is shear strain rate. Shear stresses were converted to differential stresses as

$$\sigma_{diff} = 2\tau,$$
 (2)

where τ is shear stress and σ_{diff} is the differential stress as all forcing blocks were pre-cut at 45° to the principal stress, σ_1 .

The compiled data points illustrate what temperatures, confining pressures, and differential stresses are often used in experiments (Fig. 2). It is clear, that most studies to date focused on high-temperature, viscous deformation of quartzites given that the vast majority of data comes from experiments conducted at 900–1000 °C (Fig. 2c). Interestingly, almost no data exists in the temperature range of 200–500 °C (Fig. 2b). One reason for this gap is that quartzites are extremely strong and very hard to deform using classical constant-displacement rate experiments at these conditions. Nevertheless, this temperature range could be explored using constant-load experiments and would be very valuable for constraining high-temperature brittle creep.

The experimental data shows a bimodal distribution in terms of confining pressure with a peak at 300 MPa and a second peak around

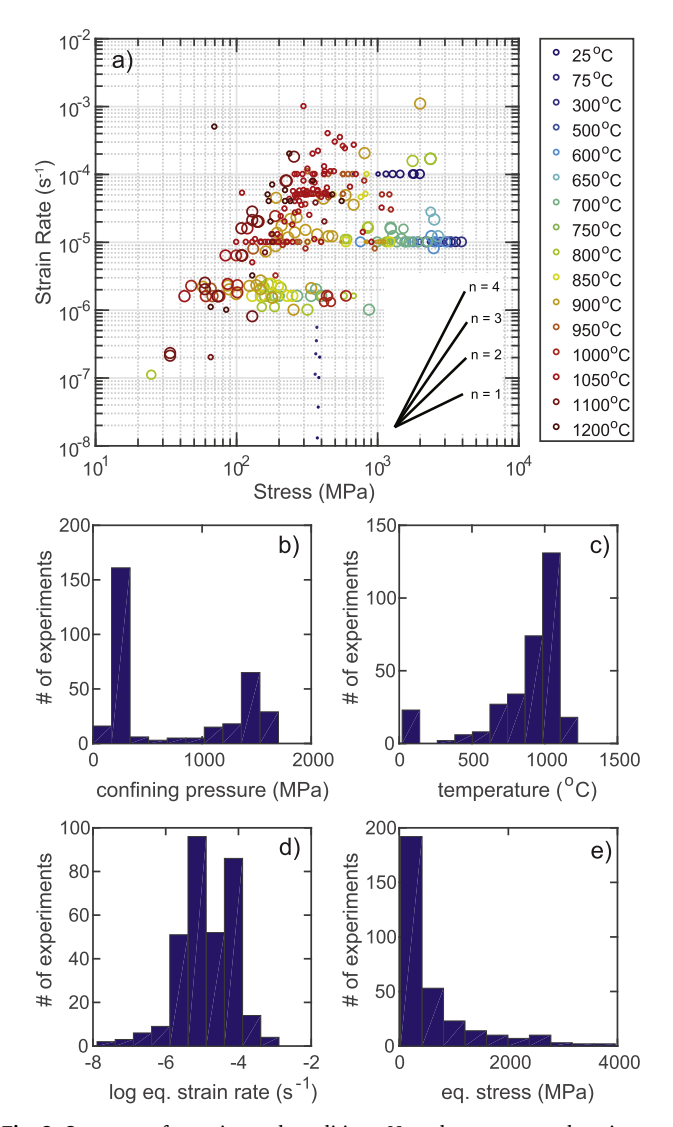


Fig. 2. Summary of experimental conditions. Note that stresses and strain rates in shear experiments have been converted into equivalent stresses and strain rates. a) All experiments in log stress, log strain-rate space. Circle size corresponds to the confining pressure where the largest symbols correlate to a confining pressure of 1.7 GPa and the smallest to 0.1 MPa, Inset shows stress exponent, n. b) Confining pressure, c) Temperature, d) Equivalent strain rate, and e) Equivalent stress. (For a color version of this figure, the reader is referred to the web version of this article.)

1500 MPa (Fig. 2b). These pressures are typical of high stress resolution gas-medium deformation apparatus studies and lower stress resolution solid-medium deformation apparatus studies. Again, a relative scarcity of data exists for confining pressures from 400 to 1000 MPa. Also, the distribution of employed equivalent strain rates shows that most experiments are conducted at typical lab strain rates of 10^{-6} – 10^{-4} s $^{-1}$ and only a few excursions to higher and lower strain rates exist (Fig. 2d). This distribution is fundamentally limited by the lifespan of an average experimentalist on the lower end and strength of quartzites with respect to deformation apparatuses on the upper end.

As discussed in the introduction, the transition from brittle to viscous deformation is expected to be marked by a decrease in the pressure sensitivity of peak strength due to the suppression of dilatant cracking and promotion of volume-conserving viscous flow. Considering the experimental data for pressure sensitivity of differential stress as a function of temperature, experiments below 600 °C exhibit a positive pressure dependence of differential stress with a differential stress to confining pressure ratio of approximately 2 (Fig. 3). This value drops

sharply and abruptly at $650\,^{\circ}\text{C}$ where experiments display no, or a slightly negative pressure dependence of stress (Fig. 3b). This abrupt change indicates that the experiments become confining pressure insensitive at the employed strain rate, so that viscous deformation dominates.

3. Model description

The three flow laws that we use were all developed for wet conditions and a quartz mineralogy (Table 1). However, the input conditions used to derive the individual flow laws differ significantly. The brittle-creep flow law was benchmarked with experimental data obtained from a low porosity sandstone. The parameters for the dislocation-creep flow law were derived from experiments on natural quartzite whereas the dissolution-precipitation flow law was derived from experiments performed on hot-pressed quartz aggregates. All the flow laws are derived for slow strain rates $(10^{-5}-10^{-8})$ and the same mineral phase. Note that the difference in experiment material leads to differences in porosity, purity, and crystal size and distribution which allows only for a limited comparability of the data.

3.1. Brittle creep

In the presence of water, fractures can propagate even when the stress intensity factor is smaller than the fracture toughness of the rock ($K_{\rm I} < K_{\rm IC}$) due to stress corrosion. This behavior allows fractures to grow and rocks to fail at stresses well below their short-term failure strength while experiencing constant applied stresses leading to 'brittle creep'.

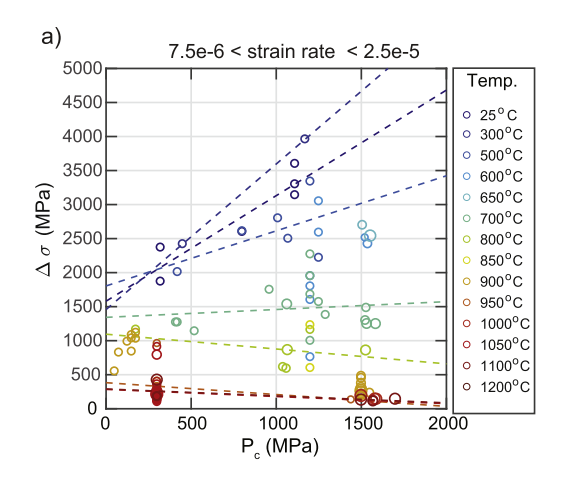
We use a brittle creep law developed by Brantut et al. (2012), based on work by Ashby and Sammis (1990) (Table 1). For a complete derivation of all the equations please refer to Brantut et al. (2012) and references therein. We consider all compressional stresses to be positive. σ_1 is the principal stress and $\sigma_2 = \sigma_3$ are the confining stresses.

The brittle-creep flow law describes the strain rate during secondary creep due to the growth of wing cracks (mode I fractures) from pre-existing mode II fractures (Fig. 4). The pre-existing fractures are all oriented at an angle Ψ to σ_1 , where $\Psi=\pi/4$, which is a favorable orientation for sliding on these fractures. The nucleation and propagation of wing-cracks parallel to σ_1 is the agent of brittle deformation, leading to a dominant set of micro fractures.

To formulate a flow law for secondary creep describing the macroscopic strain rate due to subcritical crack growth under constant differential stress and overall compression, Brantut et al. (2012) coupled a sliding wing-crack model developed by Ashby and Sammis (1990) with Charles' law (1958) of subcritical crack growth (Table 1). The flow law takes the form

$$\dot{\varepsilon} = e^{-H/RT} \left[1 - k \frac{\sigma_{peak} - \sigma_1}{\kappa_{IC}/\sqrt{\pi a}} \right]^{n+1}$$
(3)

where $\dot{\varepsilon}$ is the strain rate, H is the activation enthalpy, R is the gas constant and T temperature in Kelvin. $K_{\rm IC}$ is the fracture toughness for mode I fractures and σ_{peak} is the short term strength of the rock. n is the corrosion index and a is the initial fracture length. k is a non-dimensional numerical factor that is dependent on the wing crack length l, pre-existing fracture length a, friction coefficient μ , and a fitting parameter β , necessary for the equation to hold in 3D and for small fracture length (Brantut et al., 2012). Using a typical friction coefficient of $\mu=0.7$ and allowing the maximum wing crack length not to exceed the length of the initial fracture a, as well as approximating $\beta\sim 1$, k will be about 0.1 (Brantut et al., 2012). For simplicity, we will use this approximation in our calculations. Following the model developed by Ashby and Sammis (1990), a wedging force can be derived that couples σ_1 and σ_3 , and controls the mode I stress-intensity factor, $K_{\rm I}$ at the tip of an opening wing crack. $F_{\rm w}$ is the sliding force acting parallel to the



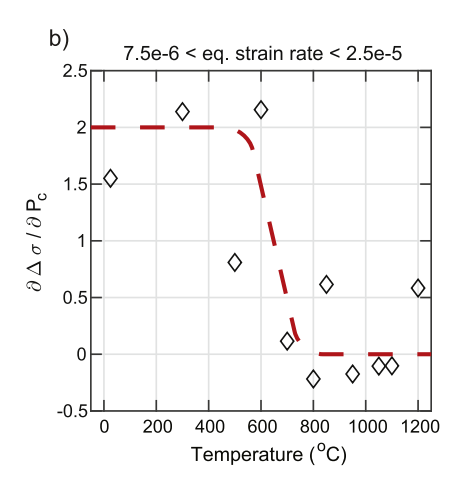


Fig. 3. Pressure sensitivity of differential stress in experiments conducted at strain rates of $\approx 10^{-5} \ s^{-1}$ a) Confining pressure, Pc vs. differential stress, σ . Dashed lines show least-square fits through the data. Note the positive pressure dependence at low temperatures and the slightly negative pressure dependence at high temperatures. b) First derivative of stress by confining pressure (i.e. slope of best fit lines in a)) vs. temperature. Notice the abrupt change in pressure dependence at 650 °C. See Appendix for the references to the experiments. (For a color version of this figure, the reader is referred to the web version of this article.)

 Table 1

 Compilation of used flow laws and corresponding parameters.

Brittle creep	Dislocation creep	Dislocation precipitation creep
Brantut et al., 2012	Hirth et al., 2001	Rutter and Brodie, 2004
$\dot{\varepsilon} = e^{-H/RT} \left[1 - k \frac{\sigma_{peak} - \sigma_1}{K_{IC}/\sqrt{\pi a}} \right]^{n+1}$	$\dot{\varepsilon} = A f^m_{H_2O} \sigma_{diff}{}^n exp \left(\frac{-Q}{RT} \right)$	$\dot{\varepsilon} = 0.4\sigma_{\text{diff}} \exp^{(-Q/RT)}/d^2$
Parameters for Crab Orchard Sand Stone (Heap et al., 2009)	Parameters for quartzite (Gleason and Tullis, 1995)	Parameters for hot-pressed Brazilian quartz aggregates (Rutter and Brodie, 2004)
Activation enthalpy: H = 31 kJ/mol	Pre-exponent factor: $A = 1.1*10^{-4}$	Differential stress; σ_{diff} (variable)
Gas constant: $R = 8.314 \text{ J/K}$	Water fugacity: $f_{H2O} = 1$	Gas constant: $R = 8.314 \text{ J/K}$
Temperature: T (variable)	Water fugacity exponent: m = 1	Temperature: T (variable)
Numerical factor: $k = 0.1$ (value from Brantut et al., 2012)	Differential stress: σ_{diff} (variable)	Initial grain size: $d = 0.4 \mu m$
Fracture toughness: $K_{IC} = 0.45*10^6 \mathrm{Pa}\mathrm{m}^{1/2}$	Stress exponent: $n = 4$	Activation energy: Q = 200 kJ/mol
Peak stress: $\sigma_{peak} = 430 \text{ MPa}$ (at confining pressure = 30 MPa)	Activation energy: Q = 223 kJ/mol	Gas constant: $R = 8.314 \text{ J/K}$
Stress: σ ₁ (variable)	Gas constant: R = 8.314 J/K	Temperature: T (variable)
Initial flaw size: $a = 0.25*10^{-3} \mathrm{m}$	Temperature: T (variable)	-
Corrosion index: $n = 13.7$		

minimum stress direction and is dependent on the initial fracture length.

$$F_{w} = (A_{1}\sigma_{1} - A_{3}\sigma_{3})a^{2} \tag{4}$$

where

$$A_{1} = \pi \sqrt{\frac{\beta}{3}} \left[\sqrt{1 + \mu^{2}} + \mu \right] \tag{5}$$

$$\beta = \frac{1}{\pi} \frac{\sqrt{1 + \mu^2} + \mu}{\sqrt{1 + \mu^2} - \mu} \tag{6}$$

$$A_3 = A_1 \frac{\sqrt{1 + \mu^2} + \mu}{\sqrt{1 + \mu^2} - \mu} \tag{7}$$

We chose to consider this behavior for experimental data for Crab Orchard Sandstone (Heap et al., 2009), given its very low porosity (3.3%) that is comparable to low porosity (1–5%) quartzites typically used in high temperature and pressure experiments. The initial conditions for our analysis are from parameters measured for Crab Orchard Sandstone (Heap et al., 2009) with a friction coefficient (μ) = 0.7, fracture toughness (K_{IC}) = 0.45*10⁶ Pa m^{1/2}, initial flaw size (a) = 0.25*10⁻³ m, corrosion index (n) = 13.7, and activation enthalpy (H) = 31 kJ/mol (Fig. 5). The experiments were conducted at an effective pressure ($P_e = P_c - P_p$) of 30 MPa where the rocks attain a short-term peak strength of 430 MPa. The short-term peak strength is equivalent to the point of failure in experiments and can be estimated from the reported failure data (Heap et al., 2009).

The brittle-flow law that we consider only holds in a very specific differential stress environment. Assuming an initial fracture length of 0.25 mm, $K_{IC}=0.45{}^{*}10^{6}\,\mathrm{Pa}\,\mathrm{m}^{1/2}$ and a k value of 0.1, $\sigma_{peak}-\sigma_{l}$ needs to be less than ≈ 100 MPa for the solution to hold. This limitation leads to a breakdown of the flow law for small differential stresses. Stress corrosion in single mode I cracks ceases once the differential stress becomes less than ~ 0.4 to $0.5{}^{*}K_{IC}$ and hence the rock stops creeping by brittle creep (e.g. Wan et al., 1990; Brantut et al., 2012). The magnitude of the minimum differential stress for which brittle creep occurs varies as a function of effective pressure and initial fracture density (Segall, 1984).

3.2. Dislocation creep

Dislocations are line defects in the crystal structure and act as agents of deformation. Dislocation creep is a volume conserving deformation mechanism with a temperature dependent rate. A number of models have been proposed to describe the strain rate in terms of applied stress, temperature, pressure, water fugacity and other external and internal variables. Here, we use the well-established power-law flow law for dislocation creep (Hirth et al., 2001) (Table 1)

$$\dot{\varepsilon} = A f^{m}_{H_2 O} \sigma_{diff}^{\ n} exp\left(\frac{-Q}{RT}\right) \tag{8}$$

where A is a pre-exponential factor, $f_{\rm H20}$ is water fugacity, m is water fugacity exponent, n is the stress exponent, and Q is the activation energy. R and T are the universal gas constant and temperature in Kelvin, respectively.

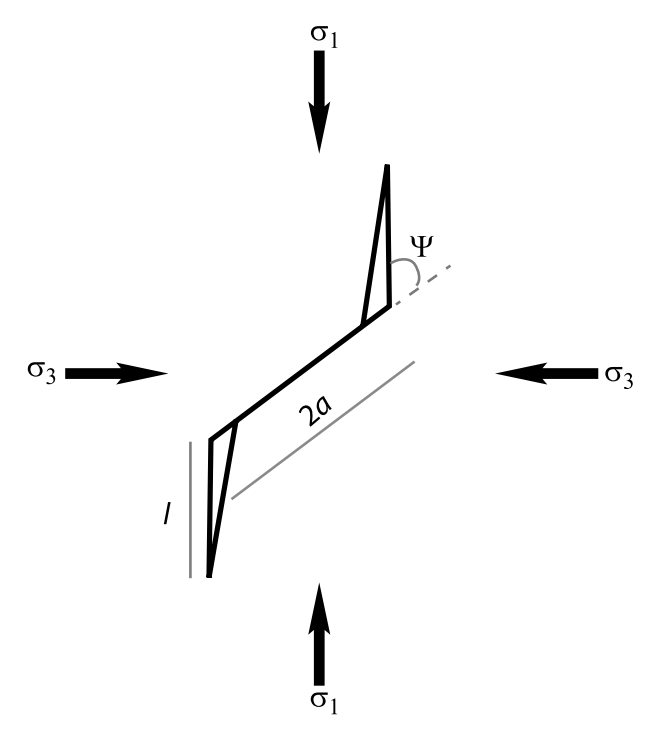


Fig. 4. Schematic setup for the brittle-creep flow law. All pre-existing fractures are at an angle, Ψ to σ_1 . l – wing-crack length, a – initial flaw length (after Ashby and Sammis, 1990 and Brantut et al., 2012).

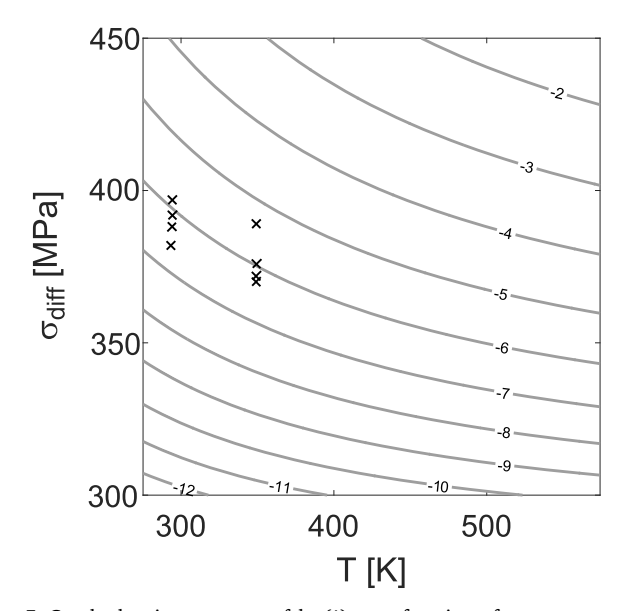


Fig. 5. Graph showing contours of $\log(\dot{\epsilon})$ as a function of temperature and differential stress for Crab Orchard Sandstone using m = 0.7, Kic = 0.45*10^6 Pa m^{1/2}, a = 0.25*10^-3 m, n = 13.7, H = 31 kJ/mol. The black crosses show data points measured by Heap et al. (2009). The measured strain rates vary between $10^{-6.3}$ and 10^{-8} .

To validate our calculated strain rate map we used the published experimental data by Gleason and Tullis (1995) and plotted 18 measured data points onto the strain rate map. The measured data points deformed at strain rates between $10^{-5.8}$ s⁻¹ and $10^{-4.1}$ s⁻¹ (Fig. 6).

3.3. Dissolution precipitation creep

Dissolution-precipitation creep is a stress-driven mass-transfer deformation mechanism that is expected to dominate at low pressures and temperatures close to the earth's surface. It is commonly in competition

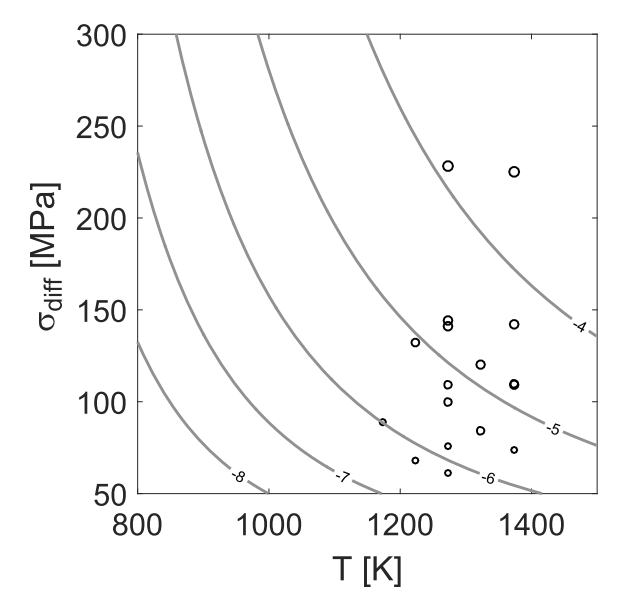


Fig. 6. Graph showing contours of $\log(\dot{z})$ of the dislocation power-law flow law as a function of temperature and differential stress. We used parameter values for Black Hill quartzite (Gleason and Tullis, 1995). A = $1.1*10^{-4}$, n = 4, H = $223 \, \text{kJ/mol}$. The black circles represent experimental data points from Gleason and Tullis (1995) with measured strain rate exponents n between -4.1 and -5.8.

with cataclasis and typically operates over longer timescales than cataclasis (e.g., Gratier et al., 1999). Solid material dissolves in the presence of its solution fluid at the point of non-hydrostatic stress. Dissolution-precipitation creep consists of three steps: 1) dissolution of mineral into a fluid phase, 2) mass transfer in the fluid, and 3) precipitation of a mineral out of the fluid (Raj, 1982). Any of these steps can be the rate-limiting process for typical experimental and geological conditions, hence complicating the derivation of broadly applicable constitutive equations to describe dissolution-precipitation creep (see Gratier et al., 2013 for a review about dissolution precipitation creep). Furthermore, the fluid phase is treated as stationary and hence, any transport of material by fluid flow is neglected. Keeping these limitations in mind, here we use the constitutive equation derived by Rutter and Brodie (2004) for grain-size sensitive flow at 300 MPa confining pressure, where volume diffusion is the rate-limiting process (Table 1).

$$\dot{\varepsilon} = 0. \ 4\sigma_{\text{diff}} e^{(-Q/RT)}/d^2 \tag{9}$$

where d is the initial grain size in μm .

We plot the calculated strain rate map together with data points from experiments performed by Rutter and Brodie (2004). The experiments were executed at temperatures of 900–1200 °C (1173–1473 K) at a confining pressure of 300 MPa. We plotted the data obtained for an initial grain size of 0.4 μm . Depending on the stress, the measured strain rate ranges from $10^{-4.5}~s^{-1}$ to $10^{-8}~s^{-1}$ and agrees well with the flow law (Fig. 7).

4. Deformation mechanism maps

The mathematical formulations for dislocation creep, brittle creep and dissolution-precipitation creep show similarities that allow direct comparison between the three flow laws and construction of deformation mechanism maps (Ashby and Frost, 1982; Ashby, 1972). All flow laws are dependent on temperature and differential stress. Our comparison of the three flow laws is only a first-order approximation, given that for example, an important mechanism which is currently not included in the analysis is high-stress, low-temperature plasticity that is expected to interact with brittle creep. Furthermore, no experimental results are currently available that would test the different flow laws for

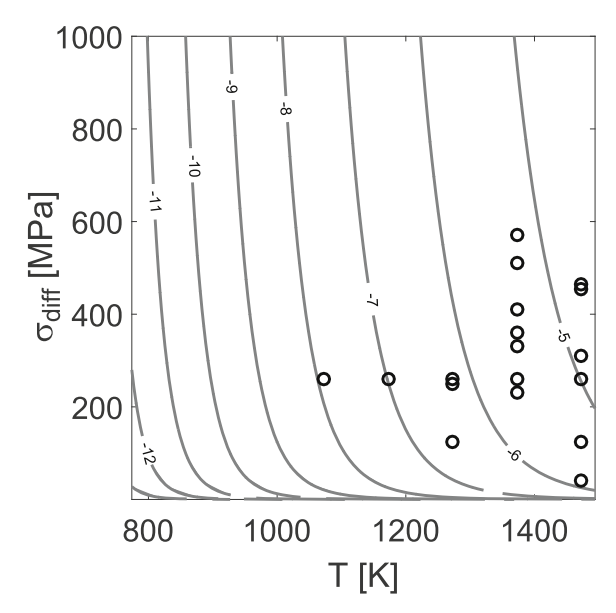


Fig. 7. Graph showing contours of $\log(\dot{\epsilon})$ of the dissolution-precipitation flow law as a function of temperature and differential stress. $d=0.4\,\mu m$. Data points (black circles) are from Rutter and Brodie (2004) and range in strain-rate exponent between -4.5 and -8.

exactly the same material. Obtaining experimental data from an identical starting material would narrow the uncertainties in the constitutive equations and would better constrain the identification of dominant deformation mechanisms for given conditions.

The deformation mechanism maps plotted in Figs. 5-7 were derived from experimental data obtained at different confining pressures. However, confining pressure is an important variable when considering deformation of rocks (e.g., Ashby and Verrall, 1977), which is not explicitly stated in constitutive equations. Confining pressure acts through water fugacity, f_{H20}^{m} , in dislocation creep, wedging force, F_{w} , in brittle creep (see section 3.1), and solubility in dissolution-precipitation creep. To achieve a more meaningful comparison between the different flow laws, we extrapolate the brittle flow law and the dislocation creep flow law to identical confining pressures. Experimental data from quartz deformation experiments at temperature below 600 °C show that the peak differential stress scales with confining pressure by about a factor of two (Fig. 3b). Even though this relationship is largely based on experiments conducted under relatively high confining pressures, the data points used for the derivation of the brittle-creep flow law fit the curve well. We use this relationship between confining pressure and differential stress to extrapolate the brittle-creep to higher confining pressures, or in other words, we increase the peak short-term strength (σ_{peak} in Eq. (3)) of the rocks as the confining-pressure increases. The confining pressure dependence of dislocation creep is expressed by the water fugacity term in Eq. (8). Given that the water fugacity exponent, m, is equal to 1 as suggested by Hirth et al. (2001), we can normalize the strain rates by the following relationship:

$$\dot{\varepsilon}_{\text{norm.}} = \left(\frac{f_{H2O}^{norm.}}{f_{H2O}^{meas.}}\right) \dot{\varepsilon}_{\text{meas.}} \tag{10}$$

where *norm.* stands for normalized and *meas.* for measured strain rate at given $f_{\rm H2O}$ conditions. To calculate the water fugacity at a given confining pressure, we use the fugacity calculator of Anthony Withers (https://www.esci.umn.edu/people/researchers/withe012/fugacity.htm).

On this basis, for a higher confining pressure, brittle creep becomes slower, which leads to a smaller domain in a deformation-mechanism map where the process is dominant (Fig. 8). This result is expected because theoretical and experimental studies on brittle creep have

shown that a lower stress limit exists. Once the differential stress drops below about 50% of K_{IC}, subcritical fracture growth stops and hence, no strain is accommodated on the fractures (Wan et al., 1990). Similarly, dislocation creep becomes slower at lower confining pressures due to the lower water fugacity. For our explored P_c -T- σ_{diff} space, brittle creep shuts down at a confining pressure of $P_c \approx 700$ MPa, leaving dislocation creep as the only active deformation mechanism. No obvious lower limit in confining pressure exists for the activity of dislocation creep. A traditional way to determine whether cracking or viscous flow processes are active is via the "Goetze's criterion", which states that cracking will be suppressed if the differential stress is of the same magnitude as the confining pressure. We see in Fig. 8 that the transition between brittle and dislocation creep occurs always at somewhat higher differential stresses than the confining pressure. However, such elevated differential stresses are commonly observed in deformation experiments which return values for stress exponent, n in the range of 3 typical of dislocation creep (e.g., Luan and Paterson, 1992), indicating that the "Goetze's criterion" is a conservative estimate for the suppression of cracking.

Also, of interest is the parameter space in a deformation-mechanism map where the two creep mechanisms significantly contribute to the deformation (Fig. 9). Using the parameters derived from experiments for a quartz mineralogy, we calculated that only a narrow temperature – differential stress band exists where both deformation mechanisms contribute significantly to the total strain rate. For these conditions, we would expect concurrent formation of fractures as well as dislocation-creep-related features. This band widens modestly for higher temperatures. Note, that this region also correlates with the area where both flow laws are less constrained due to the lack of experimental data.

To introduce dissolution-precipitation creep into the deformation mechanism-maps, we further limited the number of variables when constructing the maps. The brittle-creep and the dissolution-precipitation creep flow laws are both dependent on grain size, if in somewhat different fashion. For brittle creep, the grain size is considered to control the length of the initial flaws (Brantut et al., 2012), while for the dissolution-precipitation creep, the grain size dictates the characteristic diffusion distance (d). Both length scales can but do not necessarily have to be identical. For example, a micro-crack could comprise several grain boundaries and hence be larger than the grain size.

To construct the deformation map (Fig. 10a and b) we assume that the initial micro-fractures controlling brittle creep are three orders of magnitude larger than the grain size (characteristic diffusion distance) controlling dissolution-precipitation creep (e.g., $250 \, \mu m$ vs. $0.4 \, \mu m$).

If we assume that the initial fracture length and the characteristic diffusion distance are equal and governed by the grain size, a direct comparison between the different flow laws becomes difficult due to the coupling of fracture length and density, because small grains imply a high density of grain boundaries and hence micro-cracks. If we construct a deformation mechanism map for a large grain size (250 µm), dissolution-precipitation creep becomes very slow, to a point where it is not able to compete with the other deformation mechanisms. On the other hand, if we reduce the grain size in the brittle creep to match the grain size used to derive dissolution-precipitation creep (0.4 µm), brittle creep becomes the dominant process over the investigated stress and temperature space, due to the above-mentioned coupling of crack length and density. This result is counterintuitive given that finer grained rocks generally show higher strength in the brittle and semibrittle regime than their coarse-grained counterparts (Fredrich et al., 1990). In Fig. 10 d, we plot the deformation mechanism map for a confining pressure of 300 MPa and a grain size of 20 µm in both the brittle and the dissolution-precipitation creep. The dissolution-precipitation creep is only dominant at very low stresses over the entire range of temperature. Brittle creep is only dominant at high differential stresses over the whole temperature range.

Note that the transition between the individual deformation mechanisms is strongly dependent on the input parameters, especially the

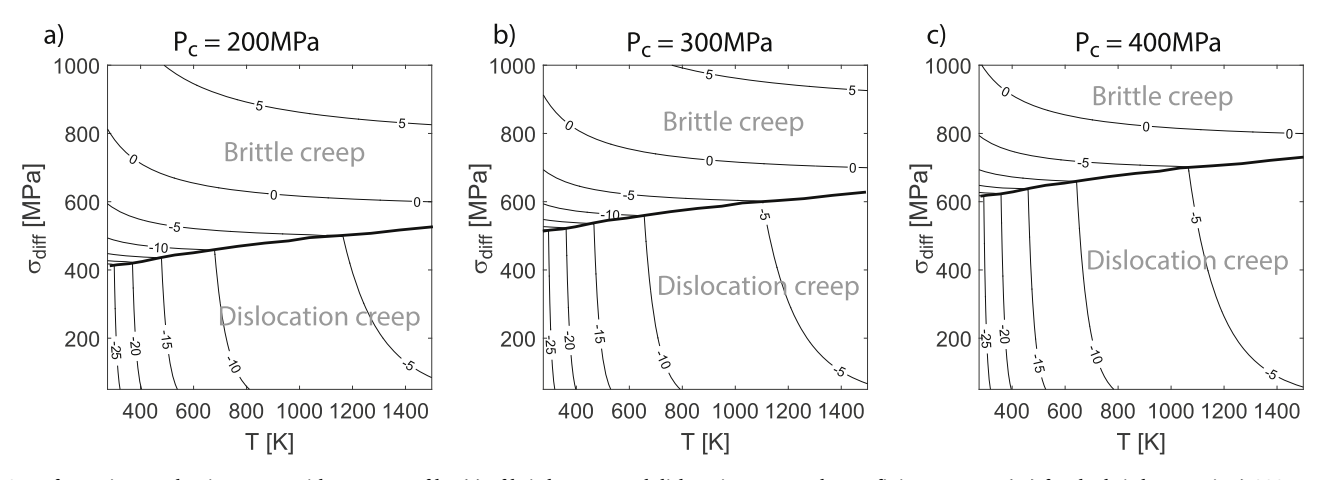


Fig. 8. Deformation mechanism maps with contours of $log(\hat{\epsilon})$ of brittle creep and dislocation creep. The confining pressure (P_c) for the brittle creep is a) 200 MPa, b) 300 MPa, and c) 400 MPa.

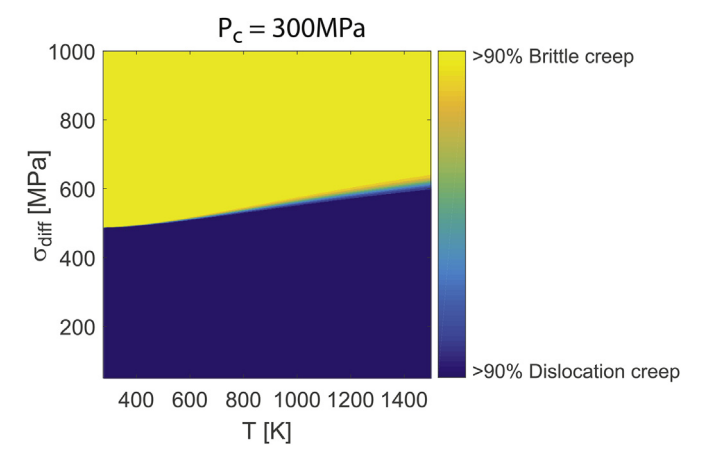


Fig. 9. Graph where yellow and blue areas represent the temperature and differential stress conditions under which brittle creep and dislocation creep, respectively, are dominant at $Pc=300\,\mathrm{MPa}$. (For a color version of this figure, the reader is referred to the web version of this article.)

grain size (i.e. crack length and characteristic diffusion distance). In Fig. 10b, the transition from brittle creep to dislocation creep is much more abrupt than the transition from dissolution-precipitation creep to dislocation creep indicating a larger parameter space where both dislocation creep and dissolution-precipitation creep, contribute significantly to deformation. This outcome is opposed to the observation of Fig. 10d where decrease in grain size broadened the transition zone between brittle and dislocation creep.

Given that brittle creep as well as dissolution-precipitation creep are dependent on grain size, (i.e. initial flaw length and density and diffusion length, respectively), we considered three grain sizes (Fig. 11). Only under conditions where sub-critical fracture growth is so slow that brittle creep comes to a halt does dissolution-precipitation creep become the dominant process. The intimate linking of initial fracture length and fracture density in the brittle creep significantly impacts the strain rate of brittle-creep and is probably not physically realistic – decoupling of the initial fracture length and fracture density would be desirable. If we assume that the initial fracture length is governed by the grain size we would expect many fractures for a small grain size, leading to very fast brittle creep. A larger grain size will lead to fewer fractures and slow down brittle creep significantly.

5. Discussion and implications

Our comparison of the existing experimentally derived flow laws for

quartz-rich rocks, shows that the calculated deformation mechanism maps are displaying an expected distribution of brittle, dislocation, and dissolution-precipitation creep as a function of temperature and differential stress. Dissolution-precipitation creep has a low activation energy and is therefore expected to dominate at low temperature, i.e. relatively shallow crustal depth. Because brittle creep breaks down at low differential stresses it dominates the deformation only at elevated differential stresses. We observe this dominance over the entire range of investigated temperatures. This observation, however, relies on the extrapolation of the brittle-creep flow law significantly past the calibrated temperature range, which is typically < 200 °C. Furthermore, as brittle creep is also strongly dependent on the number and size of the initial fractures, it can be the fastest deformation mechanism for small grain sizes where the pre-existing fractures would be expected to be quite abundant over the entire range of investigated temperatures and differential stresses (Fig. 11). Our analysis does not favor direct competition of brittle with dissolution-precipitation creep (Fig. 10) even though this competition would be expected at low temperatures and confining pressures (Gratiere et al., 1999). Note however, that grainsize reduction induced by fracturing is a necessary pre-requisite for activating dissolution-precipitation creep, highlighting the importance of serial processes in inducing semi-brittle deformation for the crust.

We note that when dealing with semi-brittle deformation, confining pressure is important, because it has a pronounced effect on brittle creep via the force acting against the opening of mode I wing cracks (e.g., Ashby and Sammis, 1990), a more modest effect on dislocation creep via water fugacity (e.g., Kronenberg and Tullis, 1984), and on dissolution-precipitation creep via quartz solubility in aqueous solution (Manning, 1994). The experimental data about dislocation creep of quartz covers a range from 300 to 1500 MPa in confining pressure (Luan and Paterson, 1992; Gleason and Tullis, 1995; Hirth et al., 2001) and hence extrapolations to lower and higher confining pressure can be made with a reasonable amount of certainty. Solubility of quartz in pure aqueous fluid is well calibrated from 0.1 to 2000 MPa confining pressure and therefore covers the whole pressure range expected in continental crust (Manning, 1994). However, brittle-creep data is available mostly at confining pressures of < 200 MPa, which makes extrapolations to higher confining pressures more uncertain. We use a simple criterion for increasing the short-term supported peak stress based on the pressure sensitivity of differential stress at low temperature (< 600 °C) using our compilation of experimental data (Fig. 3). Together with the effect of σ_3 on wing crack propagation, we can scale brittle creep to greater pressures of several hundred MPa where transition to dislocation creep could be expected in nature and experiments. Comparing our calculated deformation mechanism maps at 200-400 MPa confining pressure to that of Brantut et al. (2012) at

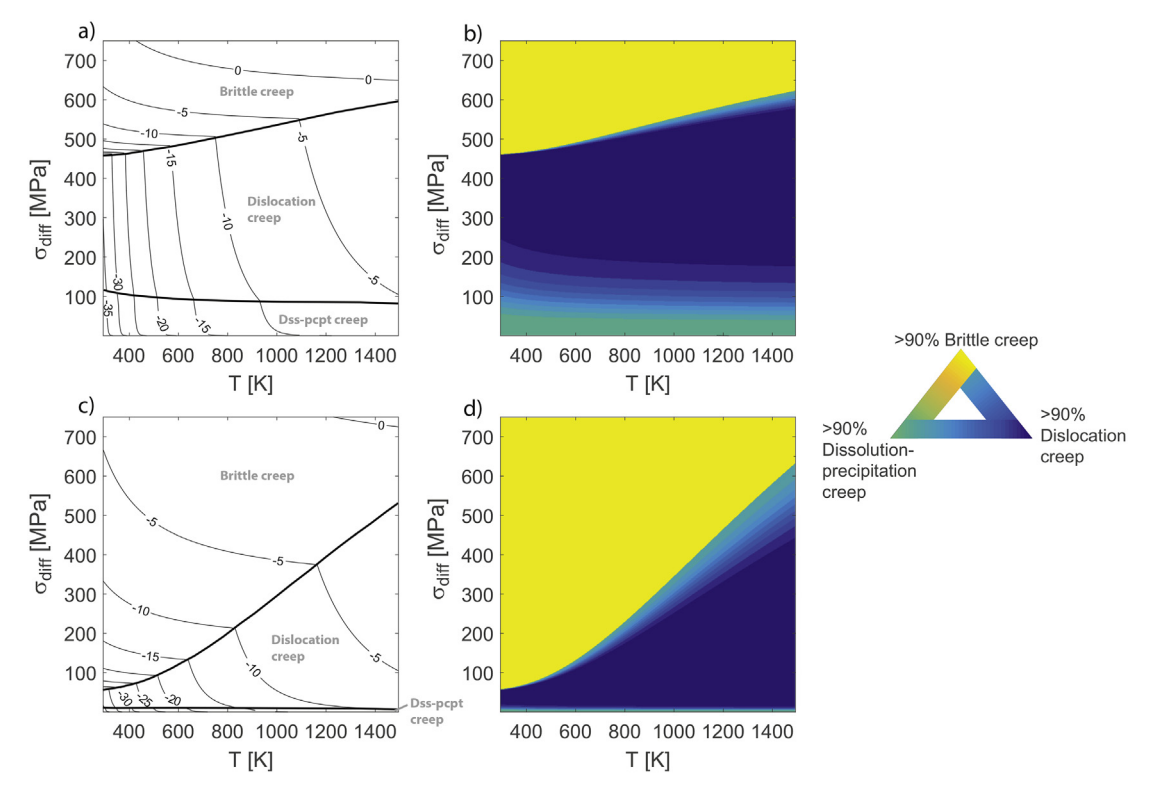


Fig. 10. a) strain rate map for brittle-, dislocation-, and diffusion creep at $Pc = 300 \, MPa$. Grain size for brittle creep = $250 \, \mu m$, Grain size for dissolution-precipitation creep = $0.4 \, \mu m$. b, d) The yellow, green and blue areas represent the temperature and differential stress conditions where brittle creep, dissolution precipitation creep and dissolution creep are dominant during deformation, respectively. c) strain-rate map for brittle-, dislocation-, and diffusion creep at $Pc = 300 \, MPa$ and grain size of $20 \, \mu m$. (For a color version of this figure, the reader is referred to the web version of this article.)

30 MPa effective pressure, we see that the field where brittle creep is dominant shrinks considerably with increasing pressure. Furthermore, the fundamental nature of brittle creep is expected to change with increasing confining pressure as mode I cracking gives progressively way to mode II cracking. This transition from mode I to mode II cracking is expected to occur between 400 and 800 MPa confining pressure (Hirth and Tullis, 1994), and hence, the validity of brittle creep models above these pressures has to be tested. Recently, Kanaya and Hirth (2017) studied semi-brittle flow of porous quartz sandstones at low effective pressures (up to 175 MPa) and high temperatures (up to 900 °C) and concluded that brittle fracturing is the main agent of deformation under these conditions. They found only a very limited contribution by dislocation glide to the total strain. These results are broadly comparable to our calculations showing that the transition from brittle creep to dislocation creep can be relatively temperature insensitive (e.g. Figs. 8

and 10a). However, this transition is also dependent on the initial fracture length and density, and will be more temperature dependent for smaller initial fracture sizes and greater fracture densities (Fig. 10d).

Examining the existing database of experiments points to a lack of data in the pressure and temperature range of 200–1000 MPa and 100–700 °C. This gap is mainly due to technical difficulties in deforming quartzites at laboratory strain rates under these conditions, however novel experiments are critical to fill in this important data gap. In Fig. 3b, we show the abrupt change in pressure dependence of differential stress at $\approx\!650\,^{\circ}\text{C}$ at strain rates of $\approx\!10^{-5}\,\text{s}^{-1}$. This transition is likely occurring due to the fact that kinetics of mass transfer responsible for viscous flow become equal or faster than the kinetics of crack growth and propagation. This mechanical transition is also accompanied by a clear microstructural change from cataclastic microstructures to mylonitic microstructures (Richter et al., 2014). If this

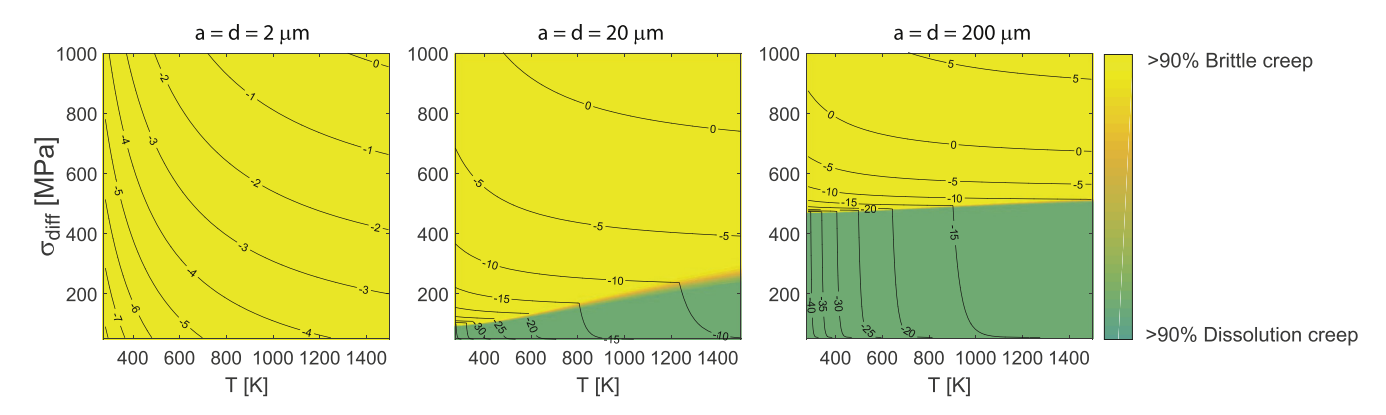


Fig. 11. Strain-rate maps for brittle and dissolution-precipitation creep at $Pc = 300 \, MPa$ for grain sizes between $2 \, \mu m$ and $200 \, \mu m$. For brittle creep, grain size = initial fracture length. The yellow and green areas show the temperature and differential stress conditions under which brittle creep and dissolution-precipitation creep are dominant. (For a color version of this figure, the reader is referred to the web version of this article.)

transition is kinetically induced, we would expect that this abrupt transition in pressure sensitivity of supported stress will be strain-rate dependent, and hence, will occur at lower temperatures for slower, geologic strain rates. Unfortunately, we do not have enough data at the moment to test this hypothesis, although the abruptness of the transition provides a good target for future experimental studies. Pinning down the strain-rate dependence of this transition would significantly aid extrapolations of experimental data to natural conditions.

Our calculations show, that with current calibrations of different flow laws only two deformation mechanisms can act in parallel and contribute to the total strain rate. However, this comparison of different flow laws has limitations and uncertainties, while being heavily dependent on extrapolating flow laws beyond conditions for which they were developed. An additional problem for the comparability is that the different flow laws are dependent on different parameters, some of which are poorly constrained and likely evolve during deformation (e.g., grain size, porosity, crack density, crack length etc.). These additional variables are kept constant in order to produce our two-dimensional contour plots. Apart from these difficulties, additional deformation mechanism(s) that are currently not constrained such as lowtemperature plasticity could be expected in the transition from lowstress dislocation creep to high-stress brittle creep. Finally, our assumption that each deformation mechanism operates independently and in parallel is a simplification. True interactions between the individual deformation mechanisms, as for example dislocation generation at crack tips (Rice, 1992), as well as serial action of individual mechanisms, as for example brittle fracturing reducing the grain sizes and hence promoting dissolution-precipitation creep, are certainly important behaviors for natural deformation (e.g., Menegon et al., 2013; Onasch, 1994; Trepmann and Stockhert, 2003). Our simplistic calculations do not account for any of these effects. Nevertheless, the deformation mechanism maps (Fig. 10b,d, 6b) show that brittle and viscous deformation mechanisms can contribute together significantly to the strain rate in a limited differential stress and temperature range. Consequently, the transition between the individual deformation mechanisms is not particularly well constrained as the flow laws have to be extrapolated over a wide temperature, differential stress, confining pressure, grain size etc. range. Furthermore, if the grain size is assumed to govern the characteristic diffusion distance as well as the crack length and density, and is held constant, brittle and dissolution-precipitation creep compete in a counter-intuitive way where fine-grained material deforms the fastest by brittle creep and dissolution precipitation cannot keep pace (Fig. 11a). Brantut et al. (2012) observe a mismatch between experimentally measured strain rates and their calculated strain rates for brittle creep. They argue that the mismatch could result from the approximation of using the grain size as the initial

Our analysis indicates that the conditions for coeval occurrence of more than one deformation behavior is limited (e.g., Figs. 9-11). This conclusion is supported by the fact that the transition in pressure sensitivity of supported stress occurs over a very narrow temperature interval of ≈50 °C in experiments (Fig. 3b). Currently the number of reported experimental observations of coeval brittle and viscous deformation processes is limited (Hirth and Tullis, 1994), although that is consistent with the limited number of experiments performed for conditions where we would expect to have the occurrence of several deformation mechanisms. However, microstructures indicative of all three investigated deformation mechanisms can be observed in natural samples of deformed quartz arenites (Onasch and Dunne, 1993; Onasch, 1994). An inherent problem with natural and experimental examples showing brittle and viscous deformation is that it is difficult or even impossible to determine whether the two different deformation mechanisms were cotemporaneous or whether the observable structures formed during cycles of brittle and viscous deformation, (Hirth and Beeler, 2015; Mancktelow, 2008; Segall and Simpson, 1986). Furthermore, it is extremely difficult to quantify the amount of strain accommodated by individual deformation mechanisms (Onasch, 1994). However, novel experimental techniques (Quintanilla-Terminel and Evans, 2016; Quintanilla-Terminel et al., 2017) make tracking of strain at high spatial resolution possible and show promise for quantifying the contribution of brittle and viscous deformation processes during semibrittle flow. Currently, it seems that the mechanical and microstructural changes accompanying semi-brittle flow of monomineralic aggregates are mostly a result of the temperature and pressure dependence of crack propagation, stress corrosion and friction rather than significant contribution of viscous deformation processes to strain accommodation (e.g. Kanaya and Hirth (2017)).

This discussion highlights the importance of understanding the deformation of polymineralic rocks in terms of semi-brittle flow. The parameter space where one mineral can accommodate strain by viscous flow whereas another mineral can accommodate strain by brittle processes will be much broader, which is a reason for why the observation of viscous deformation microstructures in quartz and brittle microstructures in feldspars is so ubiquitous in granitic mylonites in nature (e.g., Gapais, 1989; Handy, 1990; Simpson, 1985; Fitzgerald and Stünitz, 1993; Stünitz and Fitzgerald, 1993; Viegas et al., 2016). Several experimental studies on the deformation behavior of granitic rocks in the brittle (e.g., Lockner et al., 1991), semi-brittle (e.g., DellAngelo and Tullis, 1996; Pec et al., 2012a; Pec et al., 2016; Pec et al., 2012b) and viscous deformation regimes (Holyoke and Tullis, 2006a; b) are available, however the interpretation of the mechanical data is complicated by the presence of up to five mineral phases (quartz, two feldspars and two micas). Further studies on simpler, binary mixtures of minerals deforming by brittle and viscous deformation processes in the laboratory are needed to further our understanding of semi-brittle flow in terms of polyphase flow. Furthermore, models that explore the interactions between brittle and viscous processes in serial deformation are needed (Ellis and Stöckhert, 2004).

6. Conclusion

To investigate brittle-viscous flow in wet quartzites we compare brittle, dislocation, and dissolution-precipitation creep flow laws. We assume that all deformation mechanisms act independently, in parallel and can contribute to the total strain rate. The calculated strain-rate maps show a largely expected distribution of the different deformation mechanisms in differential stress and temperature space. For the comparison, we extrapolated the flow laws to equivalent confining pressures and observe the progressive diminishing of brittle creep with increasing confining pressure. The extrapolation is based on measurements of the differential stress dependence on confining pressure as derived from a compilation of rock deformation experiments. The grain size in dissolution-precipitation creep and initial fracture length in brittle creep significantly impact their co-occurrence with dislocation creep. This transition can range from abrupt to covering a range of several 100 MPas differential stress and hundreds of degrees Kelvin. A consideration of the existing collection of experimental data highlights the importance of filling current gaps between high-temperature, low stress and low-temperature, high stress deformation experiments so that quantitative flow laws for low-temperature plasticity and high-temperature brittle creep can be derived. The transition zones where more than one deformation mechanism contributes with more than 10% to the total strain rate is limited to relatively narrow differential stress and temperature conditions, dropping off sharply to where only one deformation mechanism governs the strain rate. These results suggest that semi-brittle flow will be more important in polymineralic rocks where one mineral will fracture and the other flow, as commonly observed in granitic mylonites.

Acknowledgement

We would like to thank Nicolas Brantut for helpful comments on his

work on brittle creep. Bettina Richer and an anonymous reviewer are acknowledged for helpful and constructive remarks that improved the manuscript. The detailed and very helpful comments by Editor William Dunne are gratefully acknowledged. JER would like to thank Max Reber for enlightening discussions on modeling issues. JER was supported by NSF grant EAR-1547492.

Appendix A. Supplementary data

Supplementary data related to this article can be found at http://dx. doi.org/10.1016/j.jsg.2018.05.022.

References

- Ashby, M., Frost, H., 1982. Deformation Mechanism Maps: the Plasticity and Creep of Metals and Ceramics. Pergamon Press, Oxford, UK.
- Ashby, M.F., 1972. First report on deformation-mechanism maps. Acta Metall. 20 (7),
- Ashby, M.F., Hallam, S.D., 1986. The failure of brittle solids containing small cracks under compressive stress states. Acta Metall. 34 (3), 497–510.
- Ashby, M.F., Sammis, C.G., 1990. The damage mechanics of brittle solids in compression. Pure Appl. Geophys. 133 (3), 489-521.
- Ashby, M.F., Verrall, R.A., 1977. Deformation maps for olivine. Trans. Am. Geophys. Union 58 (6) p. 512-512.
- Bhat, H.S., Rosakis, A.J., Sammis, C.G., 2012. A micromechanics based constitutive model
- for brittle failure at high strain rates. J. Appl Mech.Trans. Asme 79 (3).
 Brantut, N., Baud, P., Heap, M.J., Meredith, P.G., 2012. Micromechanics of brittle creep in rocks. J. Geophys. Res. Solid Earth 117.
- Brantut, N., Heap, M.J., Meredith, P.G., Baud, P., 2013. Time-dependent crackling and brittle creep in crustal rocks: A review. J. Struct. Geol. 52, 17-43.
- Charles, R.J., 1958. Static fatique of glass 1. J. Appl. Phys. 29 (11), 1549-1553.
- Coble, R.L., 1963. A model for boundary diffusion controlled creep in polycrystalline
- materials. J. Appl. Phys. 34 (6), 1679.
 Davis, G.H., Reynolds, S.J., Kluth, C.F., 2012. Structural Geology. Wiley.
 DellAngelo, L.N., Tullis, J., 1996. Textural and mechanical evolution with progressive strain in experimentally deformed aplite. Tectonophysics 256 (1-4), 57-82.
- Ellis, S., Stöckhert, B., 2004. Elevated stresses and creep rates beneath the brittle-ductile transition caused by seismic faulting in the upper crust. J. Geophys. Res. Solid Earth 109 (B5).
- Evans, B., 2005. Creep Constitutive Laws for Rocks with Evolving Structures. Geological Society, London, pp. 329-349 Special publication, 245.
- Fagereng, A., Hillary, G.W.B., Diener, J.F.A., 2014. Brittle-viscous deformation, slow slip, and tremor. Geophys. Res. Lett. 41 (12), 4159–4167.
- FitzGerald, J., Stünitz, H., 1993. Deformation of granitoids at low metamorphic grade. I: reactions and grain size reduction. Tectonophysics 221 (3-4), 269-297
- Fredrich, J.T., Evans, B., Wong, T.F., 1990. Effect of grain size on brittle and semibrittle strength: implications for micromechanical modelling of failure in compression. J. Geophys. Res. Solid Earth 95 (B7), 10907-10920 Wiley Online Library
- Fusseis, F., Handy, M.R., 2008. Micromechanisms of shear zone propagation at the brittle-viscous transition. J. Struct. Geol. 30 (10), 1242-1253.
- Gapais, D., 1989. Shear structures within deformed granites mechanical and thermal indicators. Geology 17 (12), 1144-1147.
- Gleason, G.C., Tullis, J., 1995. A flow law for dislocation creep of quartz aggregates determined with the molten-salt cell. Tectonophysics 247 (1-4), 1-23.
- Gratier, J.-P., Renard, F., Labaume, P., 1999. How pressure solution creep and fracturing processes interact in the upper crust to make it behave in both a brittle and viscous manner. J. Struct. Geol. 21 (8), 1189–1197.
- Gratier, J.P., Dysthe, D.K., Renard, F., 2013. The role of pressure solution creep in the ductility of the Earth's upper crust. In: In: Dmowska, R. (Ed.), Advances in
- Geophysics, vol. 54. pp. 47–179. Handy, M.R., 1990. The solid-state flow law of polymineralic rocks. J Geophys. Res. Solid Earth Planets 95 (B6), 8647–8661.
- Handy, M.R., 1994. Flow laws for rocks containing 2 nonlinear viscous phases a phenomenological approach. J. Struct. Geol. 16 (3), 287–301.
- Heap, M.J., Baud, P., Meredith, P.G., 2009. Influence of temperature on brittle creep in sandstones. Geophys. Res. Lett. 36.
- Herring, C., 1950. Diffusion velocity of a polycrystaline solid. J. Appl. Phys. 21 (5), 437-445.
- Hirth, G., Beeler, N.M., 2015. The role of fluid pressure on frictional behavior at the base of the seismogenic zone. Geology 43 (3), 223–226. Hirth, G., Teyssier, C., Dunlap, W.J., 2001. An evaluation of quartzite flow laws based on
- comparisons between experimentally and naturally deformed rocks. Int. J. Earth Sci. 90 (1), 77–87.
- Hirth, G., Tullis, J., 1994. The brittle-plastic transition in experimentally deformed quartz aggregates. J Geophys. Res. Solid Earth 99 (B6), 11731-11747.
- Holyoke, C.W., Tullis, J., 2006a. Formation and maintenance of shear zones. Geology 34 (2), 105–108.
- Holyoke, C.W., Tullis, J., 2006b. The interaction between reaction and deformation: an experimental study using a biotite plus plagioclase plus quartz gneiss. J. Metamorph. Geol. 24 (8), 743-762.
- Jammes, S., Lavier, L.L., Reber, J.E., 2015. Localization and delocalization of deformation in a bimineralic material. J. Geophys. Res. Solid Earth 120.

- Kanaya, T., Hirth, G., 2017. Brittle to semibrittle transition in quartz sandstone: Energetics. J. Geophys. Res. Solid Earth 123, 84-106.
- Klinge, S., Hackl, K., Renner, J., 2015. A mechanical model for dissolution-precipitation creep based on the minimum principle of the dissipation potential. Proc. R. Soc. A Math., Phys. Eng. Sci. 471 (2180).
- Kohlstedt, D.L., Hansen, L.N., 2015. 2.18 Constitutive Equations, Rheological Behavior, and Viscosity of Rocks A2 - Schubert, Gerald, Treatise on Geophysics, second ed. Elsevier, Oxford, pp. 441-472.
- Kronenberg, A.K., Tullis, J., 1984. Flow strength of quartz aggreagtes grain-size and pressure effects due to hydrolytic weakening. J. Geophys. Res. 89 (NB6), 4281-4297.
- Lockner, D.A., Byerlee, J.D., Kuksenko, V., Ponomarev, A., Sidorin, A., 1991. Quasi-static fault growth and shear fracture energy in granite. Nature 350 (6313), 39–42.
- Luan, F.C., Paterson, M.S., 1992. Preparation and deformation of synthetic aggregates of quartz. J Geophys. Res. Solid Earth 97 (B1), 301-320.
- Mancktelow, N.S., 2008. Interaction between brittle fracture and ductile flow during crustal deformation. Boll. Soc. Geol. Ital. 127 (2), 217-220.
- Manning, C.E., 1994. The solubility of quartz in H2O in the lower crust and upper-matle. Geochem. Cosmochim. Acta 58 (22), 4831–4839. Marti, S., Stünitz, H., Heilbronner, R., Plümper, O., Drury, M., 2017. Experimental in-
- vestigation of the brittle-viscous transition in mafic rocks interplay between fracturing, reaction, and viscous deformation. J. Struct. Geol. 105, 62–79.
- Menegon, L., Stunitz, H., Nasipuri, P., Heilbronner, R., Svahnberg, H., 2013. Transition from fracturing to viscous flow in granulite facies perthitic feldspar (Lofoten, Norway). J. Struct. Geol. 48, 95-112.
- Mott, N.F., 1951. The mechanical properties of metals. Proc. Phys. Soc. Lond. Section B 64 (381), 729–8.
- Nabarro, F.R.N., 1948. Pressure and creep tests at constant hoop stress and lead and alloy E-pipes. J. Inst. Met. 74 (12), 678-684.
- Nevitt, J.M., Warren, J.M., Pollard, D.D., 2017. Testing constitutive equations for brittleductile deformation associated with faulting in granitic rock. J Geophys. Res. Solid Earth 122 (8), 6269-6293.
- Nicolas, A., Fortin, J., Regnet, J.B., Dimanov, A., Gueguen, Y., 2016. Brittle and semibrittle behaviours of a carbonate rock: influence of water and temperature. Geophys. J. Int. 206 (1), 438-456.
- Onasch, C.M., 1994. Assessing brittle volume-grain and pressure solution volume-loss processes in quartz arenites. J. Struct. Geol. 16 (4), 519-530.
- Onasch, C.M., Dunne, W.M., 1993. Variation in quartz arenite deformation mechanisms between a roof sequence and duplexes. J. Struct. Geol. 15 (3-5), 465-475
- Pec, M., Stunitz, H., Heilbronner, R., 2012a. Semi-brittle deformation of granitoid gouges in shear experiments at elevated pressures and temperatures. J. Struct. Geol. 38, 200-221.
- Pec, M., Stunitz, H., Heilbronner, R., Drury, M., 2016. Semi-brittle flow of granitoid fault rocks in experiments. J Geophys. Res. Solid Earth 121 (3), 1677-1705.
- Pec, M., Stunitz, H., Heilbronner, R., Drury, M., de Capitani, C., 2012b. Origin of pseudotachylites in slow creep experiments. Earth Planet Sci. Lett. 355, 299–310.
- Platt, J.P., 2015. Rheology of two-phase systems: a microphysical and observational approach. J. Struct. Geol. 77, 213-227.
- Quintanilla-Terminel, A., Evans, B., 2016. Heterogeneity of inelastic strain during creep of Carrara marble: microscale strain measurement technique. J Geophys. Res. Solid Earth 121 (8), 5736-5760.
- Quintanilla-Terminel, A., Zimmerman, M.E., Evans, B., Kohlstedt, D.L., 2017. Microscale and nanoscale strain mapping techniques applied to creep of rocks. Solid Earth 8 (4), 751–765.
- Raj, R., 1982. Creep in polycrystaline aggregates by matter of transport through a liquidphase. J. Geophys. Res. 87 (NB6), 4731–4739.
- Rice, J.R., 1992. Dislocation nucleation from a crack tip an analysis based on the peierls concept. J. Mech. Phys. Solid. 40 (2), 239-271.
- Richter, B., Kilian, R., Stunitz, H., Heilbronner, R., 2014. Microstructural development of quartz gouge at the brittle-to-viscous-transition in shear experiments. Geophys. Res. Abstr. 16 EGU2014-15187.
- Rutter, E.H., 1986. On the nomenclature of mode of failure transitions in rocks Tectonophysics 122 (3-4), 381-387.
- Rutter, E.H., Brodie, K.H., 2004. Experimental intracrystalline plastic flow in hot-pressed synthetic quartzite prepared from Brazilian quartz crystals. J. Struct. Geol. 26 (2),
- Segall, P., 1984. Rate-dependent extensional deformation resulting from crack growth in rock. J. Geophys. Res. Solid Earth 89 (B6), 4185-4195.
- Segall, P., Simpson, C., 1986. Nucleation of ductile shear zones on dilatant fractures.
- Geology 14 (1), 56–59. Simpson, C., 1985. Deformation of granitic-rocks across the brittle ductile transition. J. Struct. Geol. 7 (5), 503-511.
- Stünitz, H., FitzGerald, J., 1993. Deformation of granitoids at low metamorphic grade. II: granular flow in albite-rich mylonites. Tectonophysics 221 (3-4), 299-324
- Trepmann, C.A., Stockhert, B., 2003. Quartz microstructures developed during nonsteady state plastic flow at rapidly decaying stress and strain rate. J. Struct. Geol. 25 (12), 2035-2051.
- Viegas, G., Menegon, L., Archanjo, C., 2016. Brittle grain-size reduction of feldspar, phase mixing and strain localization in granitoids at mid-crustal conditions (Pernambuco shear zone, NE Brazil). Solid Earth 7 (2), 375-396.
- Violay, M., Gibert, B., Mainprice, D., Evans, B., Dautria, J.M., Azais, P., Pezard, P., 2012. An experimental study of the brittle-ductile transition of basalt at oceanic crust pressure and temperature conditions. J Geophys. Res. Solid Earth 117.
- Wan, K.-T., Lathabai, S., Lawn, B.R., 1990. Crack velocity functions and thresholds in brittle solids. J. Eur. Ceram. Soc. 6 (4), 259–268.
- Weertman, J., 1955. Theory of steady-state creep based on dislocation climb. J. Appl. Phys. 26 (10), 1213-1217.